Effects of Drill Point Geometry on Cutting Forces and Torque When Drilling AA1050

A. Simoncelli[1,2](✉), L. Buglioni[1,3], G. Abate[1,2], P. Gayol[2], A. J. Sánchez Egea[4], and D. Martínez Krahmer[1,5]

[1] Centro de Mecánica, Instituto Nacional de Tecnología Industrial (INTI), Buenos Aires, Argentina
asimoncelli@inti.gob.ar
[2] Facultad de Ingeniería, UNLZ, Buenos Aires, Argentina
[3] Facultad de Ingeniería, Universidad de Buenos Aires, Buenos Aires, Argentina
[4] Departament d'Enginyeria Mecánica, Universitat Politècnica de Catalunya, Cataluña, Spain
[5] Instituto de Tecnología e Ingeniería, Universidad Nacional de Hurlingham, Buenos Aires, Argentina

Abstract. Reducing energy consumption in drilling operations is crucial for achieving sustainability goals. A study examined 36 drill bits with different geometries and conditions on AA1050. It assessed thrust forces and torque in two machining conditions (Cmin and Cmax) while considering mesh density, tool geometry, and boundary conditions. The results show that finer mesh models exhibit lower thrust forces, while mass scaling primarily influences torque. The pilot hole configuration decreases force, consistent with experiments. Torque decreases by increasing mesh density, matching with the experimental results. Finally, temperature and chip shape are mesh-dependent, affecting torque and force. As a result, our FEM model effectively predicted thrust force and torque, emphasizing the role of the pilot hole configuration in temperature and plastic strain results.

Keywords: Twist drill · Point geometry · Cutting forces · Computer simulation · Pilot hole

1 Introduction

Sustainability in drilling processes requires a multifaceted approach that considers four aspects [1, 2]. Firstly, the material being drilled plays a significant role. Some materials are easy to cut, while others pose challenges. Even with the possibility of using free machining elements added to the material in very small proportions, they act as tribofilms and chip breakers, facilitating chip evacuation and reducing cutting forces [3, 4]. Secondly, the cutting tool used is crucial. Coated drill bits can improve the coefficient of friction, resulting in easier chip sliding, reduced cutting forces, prevention of adhesion on contact surfaces, and decreased heat generation due to chip sliding [2]. Thirdly, lubrication is essential. Lubrication and cooling systems are employed to consume less energy and prevent tool breakage. While dry machining is the ideal technique, implementing it poses difficulties, especially in drilling aluminum and its alloys. However,

H. Kohl et al. (Eds.): GCSM 2023, LNME, pp. 668–675, 2025.
https://doi.org/10.1007/978-3-031-77429-4_74

sustainable alternatives such as compressed air or Minimal Quantity Lubricant systems exist [5]. Finally, finite element simulation methods, once validated with experimental results, prove to be an effective approach for verifying tool designs aimed at achieving minimal energy consumption [6]. Most studies focusing on drilling processes mainly address determining cutting forces based on cutting conditions and drill diameter [7], while a few consider the prediction of shear stresses in predrilling processes [8]. It is known that the drill point geometry is primarily defined by the point angle (ε), the clearance angle (α), and the web thickness (s). Each geometric variable has specific standards that provide a minimum-maximum range for their values. Since optimizing the drill geometry is a fundamental step toward developing a sustainable drilling process, dynamometric tests are done to correlate drilling forces (feed force and torque) with the drill point geometry.

This work introduces several innovations in the field of machining and drilling modeling. Firstly, it explores no-conventional geometric conditions of the tooltip (α, ε, and s) on a material of wide industrial application, including empirical tests and results, which challenge the established norms in the industry, thus opening up new possibilities and avenues for precision machining techniques. It also underscores the limited body of work dedicated to drilling with a pilot using FEM models by using a split coupled Eulerian-Lagrangian, an area that remains relatively unexplored. We are aware that a pilot hole is used to determine the constants for a mechanistic model, but it is also true that further studies are required to relate the tool geometry, material and cutting conditions.

2 Methodology

2.1 Material, Drill Bits and Drilling Conditions

The experimental drill tests were conducted on 19 mm square cross-section of AA1050 aluminum bars and material hardness of HV10 106 ± 2. Aluminum bars of approximately 400 mm in length were used during the experimental tests. A total of 72 drilling tests were done, based on combining 9 groups of drills, 4 repetitions per group and 2 cutting conditions. Consequently, 36 helical drill bits (DIN 338 helical twist drills) with a diameter of 7.5 mm were used during the experimental tests. These drills were of type N and constructed from AISI M2 high-speed steel, with the following nominal chemical composition (% by weight): 0.9% C; 6% W; 5% Mo; 4% Cr; 2% V and balance Fe. To analyze the influence of drill point geometry on drilling forces, these drills were manufactured outside the standard production program to provide four values for the clearance angle (α) (12°, 14°, 16°, and 18°), three values for the web thickness (s) (0.88 mm, 1.18 mm, and 1.38 mm), and four values for the point angle (ε) (110°, 118°, 130°, and 140°). All of these values fall within the range specified by the relevant standard for the three mentioned variables. Table 1 presents the nine tested drill groups and their associated geometries. Drilling tests were done in AA1050 with two configurations: minimum configuration (Cmin) and maximum configuration (Cmax). Cmin is defined as a 40 m/min cutting speed, 1698 rpm of spindle speed and 212 mm/min of feed speed. The Cmax is 60 m/min cutting speed, 2546 rpm of spindle speed and 318 mm/min of feed speed. All of the drilling tests were carried out in dry conditions.

Table 1. .

Drill group	Web thickness [mm]	Measured w.t. [mm]	Clearance [*]	Point [*]
G1	1.38	1.43 ± 0.02	14	130
G2	1.38	1.41 ± 0.02	14	118
G3	1.18	1.22 ± 0.02	16	118
G4	1.18	1.23 ± 0.04	14	140
G5	0.88	0.88 ± 0.02	14	118
G6	1.18	1.19 ± 0.01	14	118
G7	1.18	1.23 ± 0.04	12	118
G8	1.18	1.20 ± 0.01	18	118
G9	1.38	1.45 ± 0.10	14	110

2.2 Experimental Tests

A PROMECOR CNC milling machine with 8000 rpm and 10 kW of power was used for drilling. The machining forces were measured using a two-channel Kistler model 9271A piezoelectric dynamometer with their respective charge amplifiers, and the test data was recorded with a Labjack T7-Pro acquirer. The data processing, filtering and analysis of the signals were performed by scripts in Python programming language. All holes were drilled at a single tool depth of 10 mm (without chip withdrawal). Using the data acquirer, the torque (T) and feed force (F) signals were recorded for each drill in each test condition (Cmin/Cmax) at a sampling rate of 4 kHz. F_{RMS} and T_{RMS} average values were calculated per test with a 0.1 s window. Each signal was segmented into five equal parts corresponding to the records obtained at depths from 2.5 and 8.5 mm, to avoid transitions and filter smoothing. Table 2 shows the experimental test summary.

Table 2. .

Drill group	Thrust F max [N]	Thrust F min [N]	Torque max [Nm]	Torque max [Nm]
G1	438.7 ± 28.1	513.7 ± 33.6	0.86 ± 0.022	0.90 ± 0.023
G2	398.6 ± 20.0	430.6 ± 24.0	0.86 ± 0.026	0.89 ± 0.014
G3	373.2 ± 14.7	400.1 ± 22.2	0.84 ± 0.028	0.86 ± 0.017
G4	657.5 ± 58.3	705.7 ± 64.7	0.87 ± 0.037	0.90 ± 0.029
G5	316.4 ± 9.1	322.0 ± 14.9	0.82 ± 0.021	0.83 ± 0.010
G6	366.0 ± 18.9	394.9 ± 26.6	0.84 ± 0.024	0.85 ± 0.018
G7	378.9 ± 32.0	416.9 ± 36.4	0.84 ± 0.022	0.87 ± 0.027
G8	362.1 ± 20.09	393.8 ± 31.2	0.84 ± 0.028	0.86 ± 0.012
G9	362.1 ± 26.0	393.0 ± 24.0	0.89 ± 0.035	0.91 ± 0.031

2.3 FEM Formulation and Description

Several explicit dynamics with coupled temperature displacement FEMs have been developed in ABAQUS/Explicit to characterize the drilling process. The numerical approaches have been done in an Intel I7 10700 6-core and 12-thread CPU. These models consist of an elastic tool represented with a Lagrangian mesh (fixed with the material) and an Eulerian mixed void and material domain representing a workpiece (WP) in which material can flow through the mesh elements. This approximation of the workpiece mesh is known as Coupled Eulerian-Lagrangian and has been used before to simulate drilling processes [9, 10]. Tool geometries correspond to G4 and G5 from Table 1. For all the Eulerian cubic shape domains, the material was initially removed in a conical shape following the tip angle of the tool, in order to reduce the transient phase, such as done in [9]. Moreover, hexahedral 8 nodes and reduced integration elements were used for meshing the WP, according to [9, 10], while the tool was meshed with tetrahedrons with a higher density in the tooltip. Table 3 details model parameters, such as E_s, which stands for element length, Mass Scaling (*MS*) factor, *H* represents maximum domain height, being included the "void" space which is filled with chip formation, *Pil* represents the pilot hole configuration, and MecBC and ThBC mechanical and thermal boundary conditions tests to study influence over results. Mesh densities are detailed below group model IDs. ID 1 and 3 are the coarse mesh ones (with and without pilot hole, respectively), and specifically, ID 1 is also used for BC and MS testing, and 2 and 4 are the dense mesh models.

Table 3. Model parameters. MS and BC tests were done only with G4 tool.

Mesh ID	Tool	E_s [μm]	MS	t [ms]	H [mm]	Pil	Cond	MecBC	ThBC
1	4.5	100	100	30	3/5	No	min, max	Sides	No
1	4	100	25	30	3/5	No	max	Sides	No
1	4	100	100	30	3/5	No	max	Sides/All	No/20 °C
2	4.5	50	100	20	3	No	max	Sides	No
2	4	50	400	20	3	No	max	Sides	No
3	4.5	100	100	30	5	Yes	max	Sides	No
4	4.5	50	100	20	3	Yes	max	Sides	No

Two mesh densities have been developed and studied. The first one was adopted based on the work of [10], considering the solving time. It consists of 100 μm element length, with an initial domain total height of 5 mm, which provides sufficient clearance to maintain the chip intact. The second mesh density was adopted later when it was observed that the thrust force obtained by the model exceeded the experimental values, considering that mass scaling did not affect it. The mesh consists of 1.5 million elements for the WP, with an element length of 50 μm. In this model, consistent with the aforementioned clearance, the overall domain height has been set to 3 mm. Regarding the boundary conditions, it have been applied to the domain sides, where all displacements are fixed.

In particular, in the first model, a test was run with the bottom also fixed. Another test has been done by applying a constant temperature of 20 °C to the sides and bottom surfaces, according to [9], which constrains a convective heat transfer of the coolant. Another domain with a 2 mm pilot hole has been included to analyze the influence of this hole both in thrust force and torque. Cutting conditions Cmin and Cmax are 1698 rpm–212 mm/min and 2546 rpm–318 mm/min, respectively, and were applied as a linear function from initial time to 10 ms, to avoid oscillations. The overall runtime goes from 15 to 17 h for coarse mesh models (1 and 3) with 100x mass scaling (30 ms model time), about 22–24 h for model 1 with 25x mass scaling, and about 40 h for the dense mesh models (2 and 4) with 100x mass scaling (20 ms model time) and 20 h for the 400x mass scaling dense mesh models. Tool material has been adopted as elastic carbon steel (7850 kg/m^3, 200 GPa, 0.3 of Poisson ratio, 45 W/m°C and 420 J/kg°C) and WP is assumed as AA1050 (2710 kg/m^3, 69 GPa, 0.3, 160 W/m°C and 899 J/kg°C). A plastic flow Johnson-Cook material model has been adopted for the WP:

$$\sigma = \left[A + B(\varepsilon_P)^n\right]\left[1 + Cln\left(\varepsilon_p\right)/\varepsilon_0\right]\left[1 - (T - T_0)/(T_m - T_0)^m\right]$$

The WP parameters are defined as A-110 MPa, B-150 MPa, C-0.014, ε_0-1, n-0.36, m-1, T_m-645 °C and T_0-20 °C. The proportion of heat flux produced at the contact interface that was conducted to the tool and WP is determined by a heat partitioning coefficient, which is adjusted to 0.5 (equally distributed heat). Contact between tool and workpiece is based on the Coulomb friction model, which assumes a constant friction coefficient of 0.2, following [10]. Contact conductance was kept constant at 40 kW/(m^2 K), according to [9]. Finally, 90% of the heat generated by plastic strain is converted to heat (inelastic heat fraction). Shear stress has not been limited for this contact model and the material damage has not been considered in these models.

3 Results and Discussion

The thrust forces and torque for the two machining conditions, Cmin and Cmax, are then analyzed. Figure 1 shows at left mean values of thrust force obtained from different models. All values are obtained by averaging data from 15 ms when values stabilize.

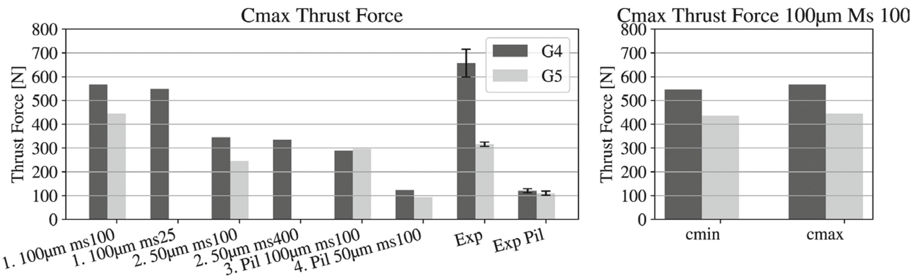

Fig. 1. Thrust force. Cmax condition (left). Cmin vs. Cmax (right).

The influence of the mesh density shows that the thrust forces are found below experimental ones in the finer mesh density models, particularly in G4 tool. Several factors could influence this low thrust force. According to [11], contact friction formulation and tool wear play a fundamental role. Among other material parameters, like Johnson Cook parameters, thermal expansion coefficient and material damage, have been neglected (although damage usually even decreases thrust force according to [9]). The second and fourth bars indicate mass scaling influence, showing that 100x is a good mass scaling selection since its results are similar to 25x (which requires 2x calculation times), even if it could be chosen a value of 400x, in particular for a finer mesh, considering solving times, and thrust force difference which is negligible. Bars with models 3 and 4 show thrust force in pilot hole configuration for the two mesh densities. For the finer mesh density, a numerical axial force is almost exactly the same value as the experimental one. It is seen that thrust force diminishes considerably in this configuration against WP without a pilot hole, due to the tool core. This is also observed in experimental measures, giving the major capacity of the model to predict this behavior. The right side of Fig. 1 shows differences in thrust force for both cutting conditions and tools for coarse mesh. It is important to note that thrust forces are smaller for Cmin conditions, whereas the experimental responses behave the opposite. However, these differences are 3.7% and 1.8% for G4 and G5, respectively, which is small considering the experimental dispersions. Figure 2 shows torque for all conditions and compares cutting conditions. The torque decreases significantly with mesh density, but in this case, those obtained from finer mesh are very similar to the experimental ones. The prediction capacity is a crucial advantage of the model, specially considering that power consumption is directly determined by torque. For all cases, G5 tool results in a greater torque than G4, but with small differences. Thrust force and torque values have also been evaluated for Cmax conditions, coarse mesh, G4 tool changing both mechanical (by adding displacement restrictions at the bottom) and thermal (by the constraining temperature at the bottom and sides to 20 °C) boundary conditions. The results seem not to be affected by these constraints. The two bars on the left show torque in the pilot configuration. Regarding the mass scaling, from 25x to 100x is an increase in torque of 7%, whereas from 100x to 400x is an overestimation of 16%. Here, the torque is almost the same with or without a hole, which is coherent with experimental observations, and it makes sense since what contributes to torque is mainly the cutting part of the tooltip. It is also denoted by a slight increase in the value from Cmin to Cmax. These variations are small, 4.5% and 1.4% for G4 and G5, respectively. One of the causes is that friction could have been underestimated and, if increased as in [9], could produce more heat in the case of Cmax due to greater rotational velocity. Another friction-sliding mechanism could be analyzed, allowing limitation of shear stress like [9, 10].

Temperatures after 19 ms are shown in Fig. 3. It is evaluated at this particular time and not when the simulation is over due to the chip shape, which rises up until it flows above and outside the upper face of the domain, losing its continuity and giving the resulting chip remains, which is difficult for a proper view. The maximum values for coarser mesh are nearly the same for each tool, at about 200 °C. Also, the mesh density has a crucial impact on both the thickness and shape of the chip, having a smaller thickness and narrow curvature in the case of finer mesh, and is directly related to the impact on both torque and thrust force. The cut chip shape in the Cmax is due to a small overall domain height and does not affect the results.

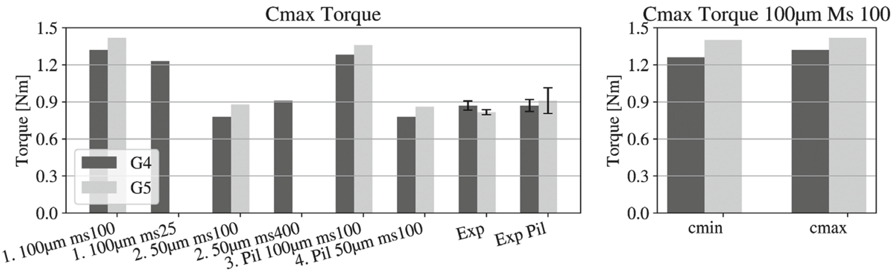

Fig. 2. Thrust force. Cmax condition (left). Cmin vs. Cmax (right).

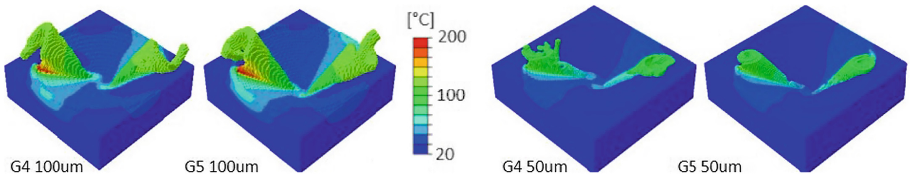

Fig. 3. Temperatures after 19 ms. Models 1 and 3. 100x MS, Cmax conditions.

Finally, the ratio of kinetic energy against internal energies should be maintained above 5%, in order to be sure that the mass scaling magnitude is not too excessive (mass scaling also affects forces, as seen before). Also, artificial energy (which is involved in solving element reduced integration) should be below 1–2% of internal energy. It is observed that the kinetic vs. internal energy relation is significantly low, about 1.3%, which has not been diminished even with finer mesh.

4 Conclusions

Several finite element models have been developed to investigate and predict outcomes in drilling processes. Various model parameters have been studied, such as mass scaling, mesh density and both thermal and mechanical boundary conditions. For most refined mesh models and considering the simplifications adopted, torque values are notoriously accurate with respect to the experimental tests. This is a major achievement of the model, bearing in mind that power consumption is directly related to torque values. The model also shows thrust force and torque extremely similar for the pilot hole configuration, in which the influence of the tool core is neglected. Another major capacity of the model is the prediction of magnitudes that are difficult or even impossible to measure, such as temperature or plastic strain.

References

1. Pervaiz S, Kannan S, Kishawy HA (2018) An extensive review of the water consumption and cutting fluid based sustainability concerns in the metal cutting sector. J Clean Prod 197:134–153

2. Astakhov VP (2014) Drills: science and technology of advanced operations
3. Krahmer DM, Urbicain G, Egea A (2020) Dry machinability analyses between free cutting, resulfurized, and carbon steels. Mater Manuf Process 35(4):460–468
4. Krahmer DM, Hameed S, Sánchez Egea AJ (2019) Wear and MnS layer adhesion in uncoated cutting tools when dry and wet turning free-cutting steels. Metals 9(5)
5. Berzosa F, Rubio EM, Agustina B, Davim JP (2020) Geometric optimization of drills used to repair holes in magnesium aeronautical components. Metals 10(11)
6. Pervaiz S, Samad WA (2021) Drilling force characterization during Inconel 718 drilling: a comparative study between numerical and analytical approaches. Materials 14:4820
7. Tamura S, Matsumura T (2022) Cutting force in drilling with flat bottom drill. Key Eng Mater 926:1636–1642
8. Kim KS (2015) Analysis of drilling of a metal plate with pilot hole. Arch Metall Mater 60(2):1–4
9. Priest J, Ghadbeigi H, Avar S (2021) 3D finite element modelling of drilling: the effect of modelling method. J Manuf Sci Technol 35:158–168
10. Abdelhafeez AM, Soo SL, Aspinwall D (2016) A coupled Eulerian Lagrangian finite element model of drilling titanium and aluminium alloys. CIRP J Manuf Sci Technol 9:198–207
11. Laakso SVA, Agmell M, Ståhl J-E (2018) The mystery of missing feed force – the effect of friction models, flank wear and ploughing on feed force in metal cutting simulations. J Manuf Process 33:268–277